



Phosphoregulation of DNA repair *via* the Rad51 auxiliary factor Swi5–Sfr1

Received for publication, March 9, 2023, and in revised form, June 6, 2023 Published, Papers in Press, June 16, 2023,
<https://doi.org/10.1016/j.jbc.2023.104929>

Pengtao Liang[†], Katie Lister[†], Luke Yates, Bilge Argunhan^{*†}, and Xiaodong Zhang^{*†}

From the Section of Structural and Synthetic Biology, Faculty of Medicine, Imperial College London, London, UK

Reviewed by members of the JBC Editorial Board. Edited by Patrick Sung

Homologous recombination (HR) is a major pathway for the repair of DNA double-strand breaks, the most severe form of DNA damage. The Rad51 protein is central to HR, but multiple auxiliary factors regulate its activity. The heterodimeric Swi5–Sfr1 complex is one such factor. It was previously shown that two sites within the intrinsically disordered domain of Sfr1 are critical for the interaction with Rad51. Here, we show that phosphorylation of five residues within this domain regulates the interaction of Swi5–Sfr1 with Rad51. Biochemical reconstitutions demonstrated that a phosphomimetic mutant version of Swi5–Sfr1 is defective in both the physical and functional interaction with Rad51. This translated to a defect in DNA repair, with the phosphomimetic mutant yeast strain phenocopying a previously established interaction mutant. Interestingly, a strain in which Sfr1 phosphorylation was blocked also displayed sensitivity to DNA damage. Taken together, we propose that controlled phosphorylation of Sfr1 is important for the role of Swi5–Sfr1 in promoting Rad51-dependent DNA repair.

DNA damage occurs through both exogenous and endogenous sources, making it an unavoidable occurrence in the life of all organisms. The arsenal of DNA repair processes is vast and varied, but a common feature is the use of the intact complementary DNA strand as a template for synthesis-dependent repair of the damaged strand. A single DNA double-strand break (DSB) interrupts the continuity of the DNA molecule, precluding the use of the complementary strand as a template. Taken together with the fact that a single DSB is sufficient to cause cell death, DSBs pose a particularly challenging threat to the cell. Homologous recombination (HR) is a major DSB repair mechanism that circumvents the problem of disrupted continuity by identifying another region in the genome that shares high sequence identity (*i.e.*, homology) to the damaged DNA and utilizing this region as a template for synthesis-dependent repair (1).

The DNA ends at a DSB site are processed by nucleases to generate 3'-ended single-stranded DNA (ssDNA) tails that are first bound by the ssDNA-binding protein replication protein

A (RPA) (2). RPA is then replaced with the RecA-family recombinase Rad51, which oligomerizes to form a right-handed helical filament with the ssDNA running along its central axis (3). This nucleoprotein filament interrogates the genome to identify a homologous region of intact double-stranded DNA (dsDNA) and invades into the duplex DNA, displacing the identical strand and forming base-pairs with the complementary strand, leading to the formation of a key recombination intermediate known as a displacement loop (D-loop) (4, 5). The D-loop can be expanded by Rad51-driven strand-exchange and extension of the 3'-ended invading strand, which serves as a primer for DNA synthesis. The invading strand then dissociates from the duplex, and having been extended, can anneal to the ssDNA exposed on the other side of the DSB. Following gap filling by further DNA synthesis and ligation of resultant nicks, DSB repair by HR is complete. This model of HR is known as synthesis-dependent strand annealing and is strictly dependent on Rad51 (1). Thus, the formation/stabilization of the Rad51 nucleoprotein filament is highly regulated.

The Swi5–Sfr1 (S5S1) auxiliary factor complex was first identified as a Rad51 regulator in the fission yeast *Schizosaccharomyces pombe* (6). Biochemical reconstitutions with purified proteins directly demonstrated that S5S1 physically interacts with Rad51 and stimulates its strand exchange activity by stabilizing Rad51 nucleoprotein filaments (7, 8). Homologues have since been identified in mice and humans (9, 10), and experiments with mouse proteins indicated that the mechanisms underlying Rad51 potentiation by S5S1 are largely conserved (11–14).

Structural analysis of *S. pombe* S5S1 demonstrated that it is an elongated heterodimer: the crystal structure of the C-terminal half of Sfr1 in complex with Swi5 (S5S1C) revealed that this truncated complex forms a coiled-coil, whereas the N-terminal half of Sfr1 (Sfr1N) was shown to be intrinsically disordered by circular dichroism (CD) spectroscopy and nuclear magnetic resonance analysis (15–17). These two structurally distinct domains were also found to comprise disparate functional modules (16). While S5S1C could activate Rad51, ~10-fold more protein was required than wildtype (full-length S5S1) for maximal stimulation, and a S5S1C–Rad51 complex could not be detected by immunoprecipitation, suggesting that the physical interaction is very weak/transient. By contrast, Sfr1N was found to coimmunoprecipitate with Rad51 but did

[†] These authors contributed equally to this work.

* For correspondence: Bilge Argunhan, b.argunhan@imperial.ac.uk; Xiaodong Zhang, xiaodong.zhang@imperial.ac.uk.

Phosphoregulation of the Rad51 auxiliary factor Swi5–Sfr1

not stimulate Rad51 activity, leading the authors to propose that Sfr1N serves as an anchor to tether S5S1C to activate Rad51 (16). Nuclear magnetic resonance interaction analysis identified two sites in Sfr1N that bind Rad51 (17): Site 1 (Ser84–Thr114) and Site 2 (Thr152–Ser168). Mutation of seven Lys/Arg residues in these sites to Ala (S5S1-7A) severely impaired the physical and functional interaction between S5S1 and Rad51 (17).

Although the underlying molecular mechanisms are only just being elucidated, the regulation of HR by auxiliary factors has long been appreciated (18). By contrast, the role of post-translational modifications (PTMs), which represent an additional layer of regulation, is poorly understood. Although modern proteomics studies have identified many PTMs of HR auxiliary factors, how such modifications affect HR is not clear, despite increasing evidence suggesting that they are important (19). Phosphoproteomics identified multiple phosphorylated residues located in Sfr1N (20–24): S24, T73, S109, S116, S165. Interestingly, several of these are situated in/around the Rad51 interaction sites.

Here, we investigated the possibility that phosphorylation of Sfr1 regulates the interaction of S5S1 with Rad51. Mutation of the five S/T residues to phosphomimetic D residues severely impaired the binding of S5S1 to Rad51. Furthermore, the stabilization of Rad51 filaments by S5S1 was compromised by the phosphomimetic mutations, and this translated to a substantial reduction in the stimulation of Rad51-driven strand exchange. Importantly, these defects were comparable in magnitude to the S5S1-7A mutant, a bonafide interaction mutant (17). Yeast strains expressing phosphomimetic mutants of Sfr1 phenocopy *sfr1-7A*, displaying the same DNA damage sensitivity as *sfr1Δ* only in the absence of the Rad55–Rad57 auxiliary factor complex. Interestingly, cells expressing a nonphosphorylatable version of Sfr1 (five S/T to A mutations) also displayed DNA damage sensitivity, despite this mutant protein being biochemically comparable to wildtype. Taken together, we propose that phosphorylation negatively regulates the interaction of S5S1 with Rad51, providing a means to fine-tune Rad51 potentiation by S5S1.

Results

Biochemical characterization of S5S1 mutant variants

To investigate if phosphorylation of Sfr1 is pertinent to the function of S5S1 in HR, we mutated several phosphorylation sites of Sfr1 and purified the protein in complex with Swi5 (Fig. 1, A and B). Since the proteins were purified from *Escherichia coli*, wildtype S5S1 serves as the unphosphorylated sample. A variant in which five S/T residues were mutated to the phosphomimetic D residue serves as a proxy for the phosphorylated sample (S5S1-PM, phosphomimetic). Given that several of these S/T residues are situated in/around the two Rad51 interaction sites within Sfr1N (17) (Fig. 1A), any defects observed for S5S1-PM could be explained by the loss of S/T residues that are important for the interaction with Rad51. To control for this, we also purified a variant in which the S/T residues of interest were mutated to A (S5S1-NON,

nonphosphorylatable). Finally, a previously established Rad51 interaction mutant was also purified for comparison (17) (S5S1-7A, 7 K/R residues mutated to A). Consistent with the fact that the C-terminal half of Sfr1 is important for complex formation with Swi5 (16), the oligomeric state of the S5S1 heterodimer was not affected by any of these mutations in the N-terminal domain (Fig. 1C).

S/T residues located in intrinsically disordered domains are commonly targeted for phosphorylation, and in some cases, these phosphorylation events promote folding into structured domains (25, 26). To examine whether the phosphorylation of Sfr1 might alter its structure, CD spectroscopy was employed to obtain a coarse readout of global S5S1 structure. The CD spectrum of S5S1 resembled an average of disordered and α -helical signals (Fig. 1D) (27), as expected from the disordered Sfr1N and predominantly coiled-coil nature of S5S1C (16, 17). The spectra of other mutants examined here were essentially identical, suggesting that the introduction of phosphomimetic mutations does not cause any obvious change in the structural landscape of S5S1. However, the presence of S5S1C could mask any subtle changes in the disordered state of Sfr1N. We therefore purified Sfr1N and a version containing the phosphomimetic mutations (Sfr1N-PM) (Fig. 1B). Sfr1N and Sfr1N-PM both show similar elution profiles from size-exclusion chromatography (Fig. 1E), and their CD spectra were characteristic of a disordered protein (27) (Fig. 1F), as was previously observed for wildtype Sfr1N (17). These experimental data are consistent with predicted structural models of both S5S1 and S5S1-PM generated by AlphaFold (28), which show that Sfr1N of both complexes is expected to be completely disordered, except for a short α -helix at the extreme C terminus of the disordered domain (P166–C170) (Fig. 1G). Taken together, these results indicate that the global structure of S5S1 or the disordered state of Sfr1N are not obviously altered by the introduction of phosphomimetic mutations in Sfr1N.

Phosphomimetic mutations in Sfr1 impair the binding of S5S1 to Rad51

Next, we sought to directly test whether the binding of Rad51 to S5S1 is affected by the phosphomimetic mutations in Sfr1. To this end, the hexahistidine tag at the N terminus of Sfr1 was utilized in pull-down assays. As expected, when purified Rad51 (Fig. S1A) was mixed with S5S1 and complexes were precipitated using nickel resin, a significant amount of Rad51 was seen to coprecipitate with S5S1 (Fig. 2A). By contrast, substantially less Rad51 was observed when S5S1-7A was precipitated. Strikingly, a similar reduction in the coprecipitation of Rad51 was seen when S5S1-PM was employed, and this was not the case for S5S1-NON.

Early biochemical analyses suggested that S5S1 stabilizes Rad51 filaments but does not function as a canonical mediator that directly promotes Rad51 assembly on ssDNA (e.g., Rad52 in yeast and BRCA2 in humans) (8). This was largely corroborated by more recent single-molecule experiments demonstrating that S5S1 reduces the dissociation rate of

Phosphoregulation of the Rad51 auxiliary factor Swi5-Sfr1

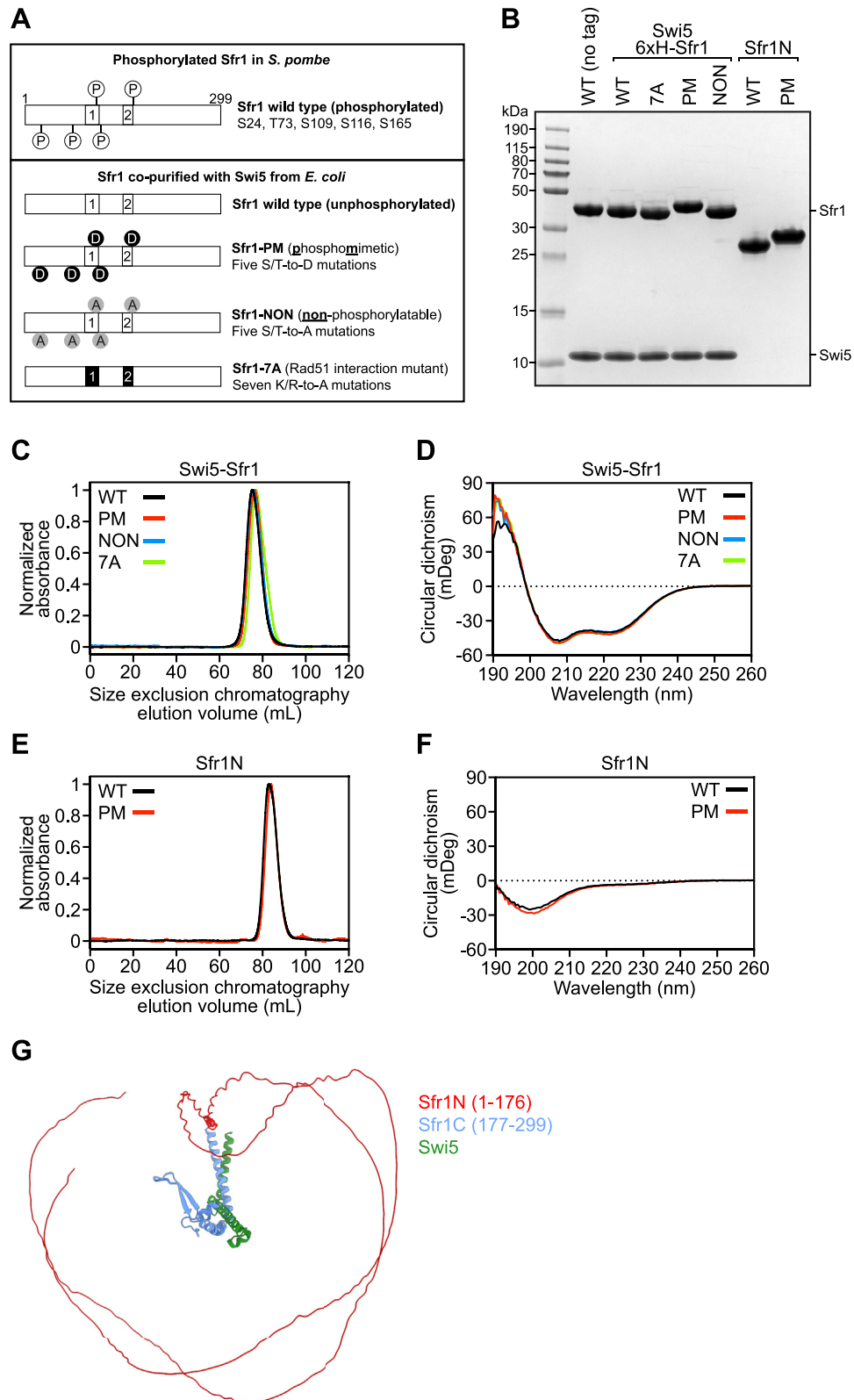


Figure 1. Biochemical characterization of Swi5-Sfr1 (S5S1) mutants. A, schematic of Sfr1 mutants. B, SDS-PAGE analysis of purified S5S1 complexes and Sfr1N variants. 2 μ g of each protein was loaded. C and E, size-exclusion chromatography analysis of indicated proteins. D and F, circular dichroism spectra of indicated proteins. G, AlphaFold models of S5S1 and S5S1-PM overlaid with Sfr1C as a reference point. Sfr1N, red. Sfr1C, blue. Swi5, green. The prediction suggests that Sfr1N remains disordered irrespective of the phosphomimetic mutations.

Phosphoregulation of the Rad51 auxiliary factor Swi5-Sfr1

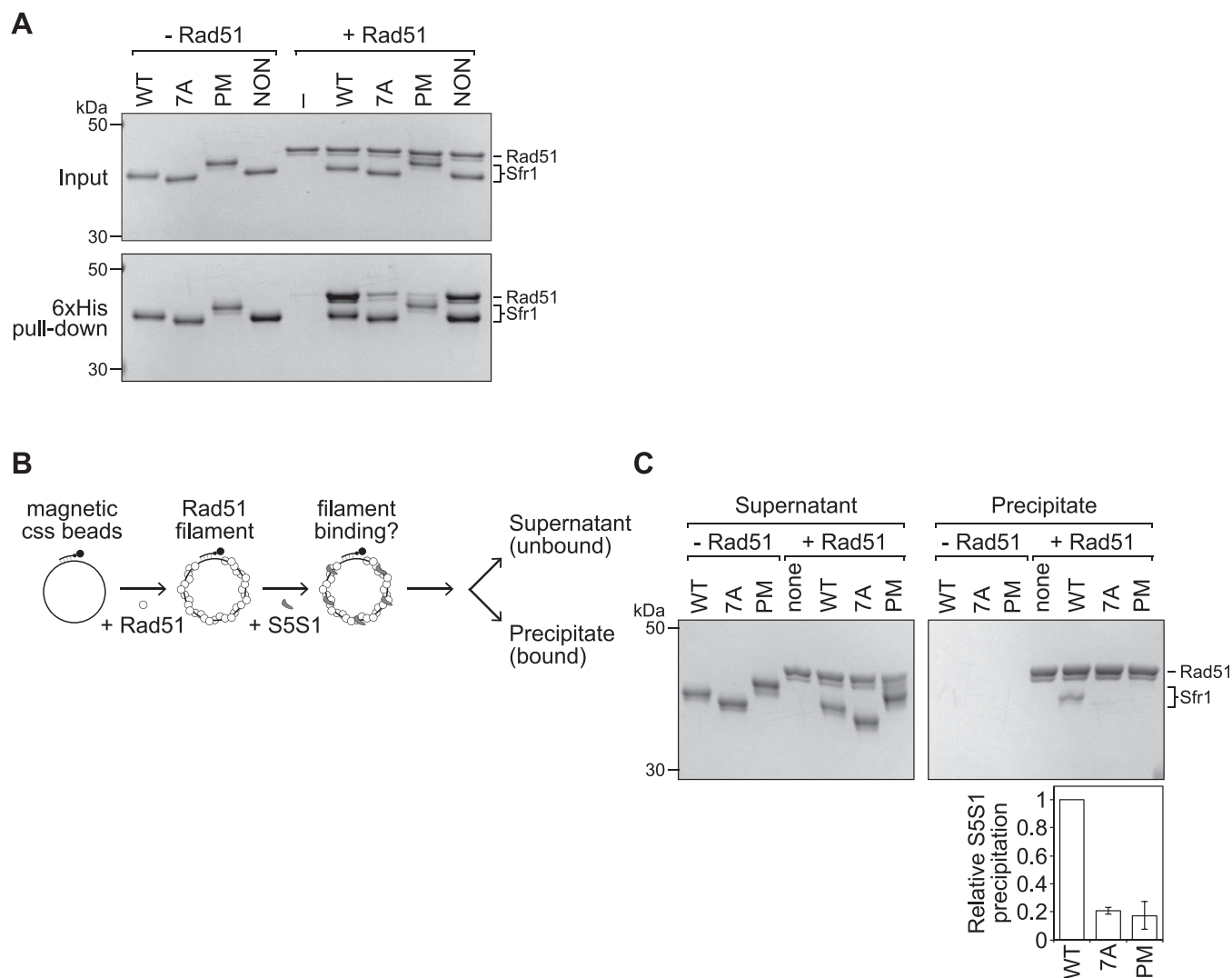


Figure 2. The physical binding of S5S1 to Rad51 is impaired by phosphomimetic mutations in Sfr1. A, pull-down experiments with nickel resin were performed with purified Rad51 and the indicated variant of hexahistidine-tagged S5S1 to examine the interaction in-solution (500 nM each protein). The content of precipitated resin from each reaction was examined by SDS-PAGE and Coomassie staining. –, protein omitted. B, schematic of the filament interaction assay. C, Rad51 filaments were pulled-down after incubation with the indicated variant of S5S1. The amount of Rad51 and Sfr1 that was precipitated was determined by SDS-PAGE and Coomassie staining. Sfr1 signal was normalized to Rad51 and expressed relative to wildtype. Averages are plotted. n = 3, error bars represent standard deviation.

Rad51–ssDNA complexes without affecting the association rate *i.e.*, S5S1 stabilizes Rad51 filaments but does not promote filament formation per se (29). We interpret these results to mean that the physiological substrate S5S1 acts on is likely to be the Rad51–ssDNA filament rather than free Rad51. With this in mind, an assay was employed to test the binding of S5S1 to Rad51–ssDNA filaments (Fig. 2B). Briefly, Rad51 filaments were formed on ssDNA that was annealed to a biotinylated oligonucleotide, and reactions were supplemented with S5S1. Following a short incubation, the Rad51–ssDNA complexes (precipitate) were separated from the unbound proteins (supernatant) using streptavidin-coated magnetic beads, and both fractions were analyzed by SDS-PAGE. Whereas a clear Sfr1 band was observed for S5S1, the Sfr1 band for S5S1-PM was barely detectable, corresponding to an approximately 5-fold reduction in the coprecipitation of S5S1 with Rad51 (Fig. 2C). A similar reduction was observed for

S5S1-7A, the established Rad51 interaction mutant (17). These results suggest that phosphorylation of Sfr1 at these five residues severely disrupts the interaction of S5S1 with Rad51.

Stabilization of Rad51 filaments is compromised by phosphomimetic mutations in Sfr1

Having determined that the physical binding of Rad51 to S5S1-PM is severely impaired, we next asked whether the magnitude of the binding defect is functionally consequential. A critical mechanism through which S5S1 potentiates Rad51 is by stabilizing Rad51–ssDNA filaments (8, 29). Although S5S1C possesses this activity, abrogation of the binding to Rad51 by mutating the interaction sites in Sfr1N (*i.e.*, S5S1-7A) severely impaired the efficiency of filament stabilization, with several-fold more protein required to effectively stabilize filaments

(16, 17). To test whether S5S1-PM can effectively stabilize Rad51-ssDNA filaments, we examined filaments by negative-stain electron microscopy (NSEM).

The formation of human RAD51-ssDNA filaments in the presence of ATP-Mg²⁺ lead to the visualization of various heterogeneous species by NSEM: short, ordered filaments; disordered filaments; and ring-like oligomers (30). We observed similar species with *S. pombe* Rad51 filaments (116-mer ssDNA) formed in the presence of ATP-Mg²⁺ (Fig. 3A). We reasoned that, under these conditions, stabilization of Rad51-ssDNA filaments by S5S1 would result in increased filament length. Indeed, longer filaments were observed upon inclusion of S5S1, and there was a concomitant reduction in other Rad51 species, indicative of improved filament stability (Fig. 3B). The addition of either S5S1-PM or S5S1-7A seemingly resulted in an intermediate state, with some longer filaments observed (Fig. 3, C and D). These qualitative observations were corroborated by measurements of filament length (Fig. 3E), which revealed that, while S5S1-PM and S5S1-7A were able to partially stabilize Rad51 filaments, they were unable to do so to the same extent as wildtype S5S1. These differences in filament stabilization were statistically significant, and the defect of S5S1-PM was indistinguishable from S5S1-7A.

S5S1 was previously shown to stabilize Rad51 filaments against disruption by Fbh1, a UvrD-family helicase that functions as an anti-recombinase in both *S. pombe* and mammals (31–33). To corroborate our NSEM results, we designed a biochemical assay to test whether S5S1-PM could stabilize Rad51 filaments against disruption by Fbh1, which constitutes a more physiologically relevant challenge (Fig. 4A). Rad51 filaments were assembled on a biotinylated ssDNA oligonucleotide (100-mer) and supplemented with S5S1 before challenging them with purified Fbh1. The ssDNA was then precipitated with streptavidin-coated magnetic beads, and the contents of the precipitate (DNA bound) and supernatant (unbound) fractions were examined by SDS-PAGE. Although Fbh1 was purified in complex with its binding partner Skp1 (Fig. S1B), which improves the solubility of Fbh1, it was previously shown that the filament disruption activity of the Fbh1-Skp1 complex is dependent on the translocase activity of Fbh1 (32), firmly establishing Fbh1 as the catalytically relevant unit in this complex. We therefore refer to this complex as Fbh1 hereafter for simplicity.

Minimal protein was precipitated in the absence of ssDNA (Fig. 4B), confirming the DNA dependency of protein precipitation. In contrast to this negligible nonspecific binding,

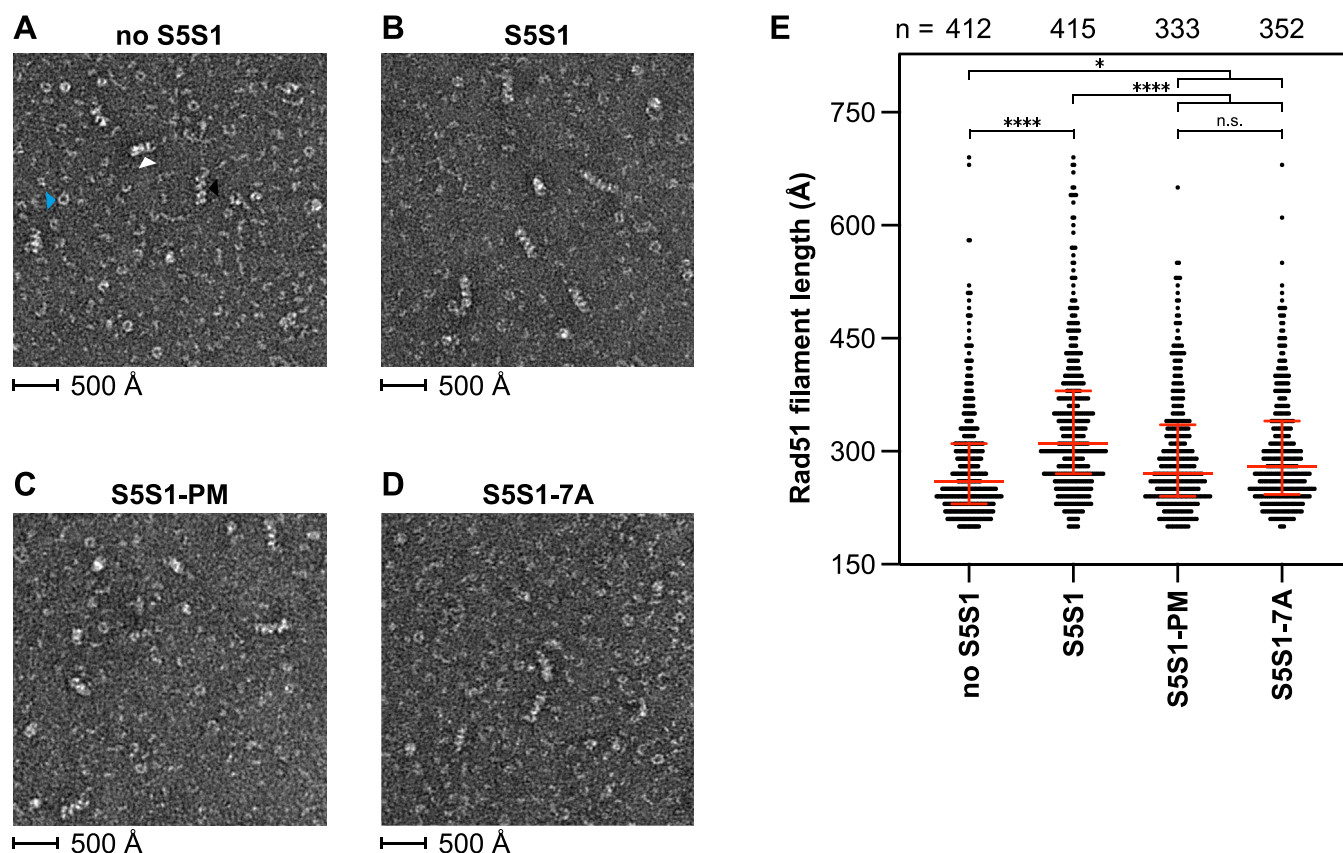


Figure 3. S5S1-PM is impaired for Rad51 filament stabilization. A–D, representative electron micrographs of Rad51 filaments formed on 116-mer ssDNA in the absence of S5S1 (A), or in the presence of S5S1 (B), S5S1-PM (C), or S5S1-7A (D). Different Rad51 species are highlighted in (A): white arrowhead, disordered filament; black arrowhead, ordered filament; blue arrowhead, ring-like oligomer. E, quantification of filament length from reactions supplemented with the indicated S5S1 variant. Red bars represent median and interquartile range. Number of filaments quantified per sample (n) is shown above the graph. One-way ANOVA with multiple comparisons correction (Tukey) was conducted to test statistical differences. * $p < 0.05$. **** $p < 0.0001$. n.s., not significant ($p = 0.9958$).

Phosphoregulation of the Rad51 auxiliary factor Swi5-Sfr1

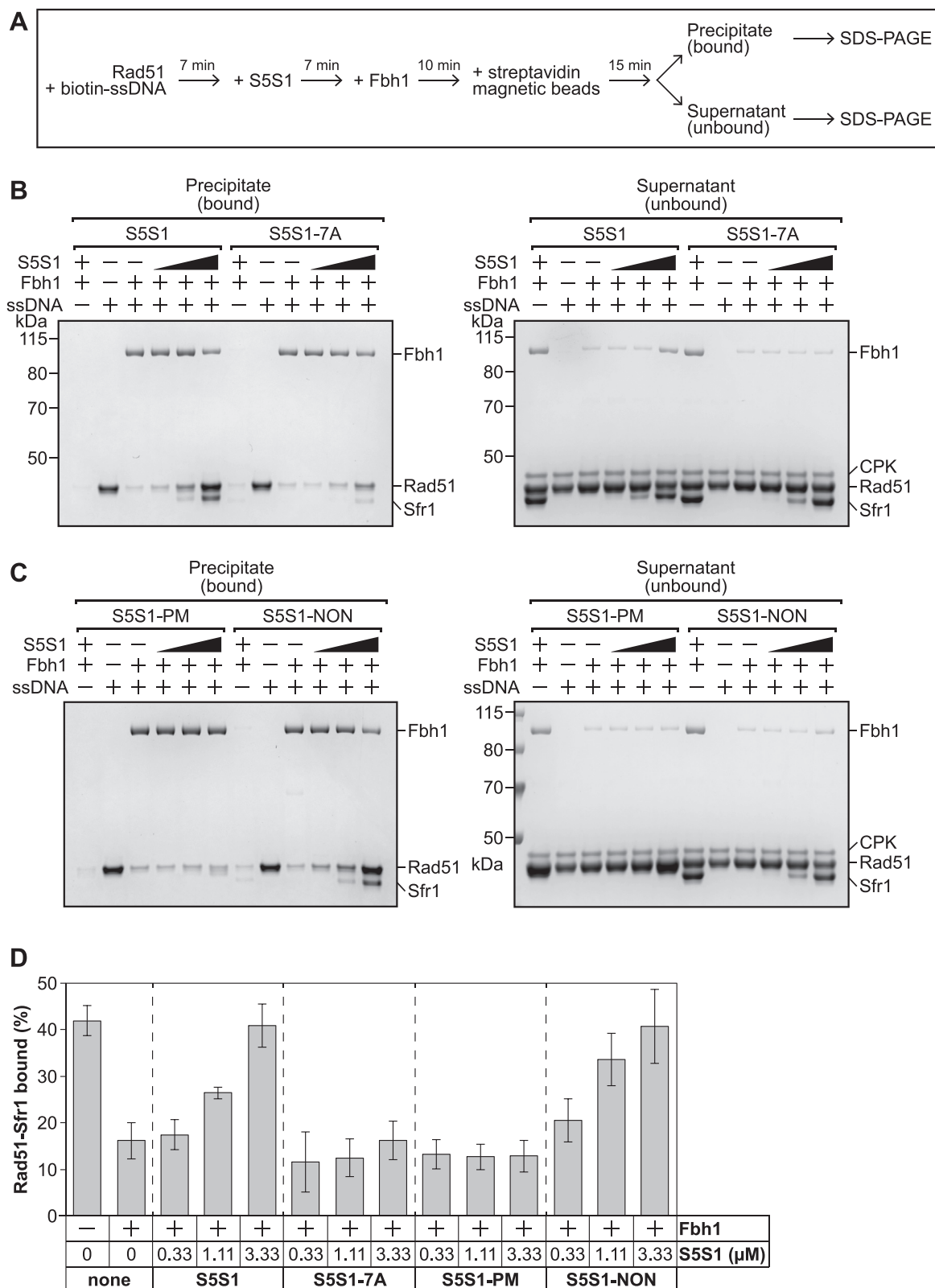


Figure 4. The Rad51-S5S1 interaction is important to antagonize Fbh1-mediated disruption of Rad51 filaments. *A*, outline of the Fbh1-mediated Rad51 filament disruption assay. *B* and *C*, experiments were conducted as depicted in (*A*). + or - indicates the inclusion or omission of protein, respectively. All incubations were at 37 °C. Rad51: 3.33 μM. Biotinylated ssDNA: 10 μM. S5S1: 0.33 μM, 1.11 μM, or 3.33 μM. Fbh1: 0.312 μM. *D*, quantification of DNA-bound Rad51. The Rad51 and Sfr1 bands were difficult to separate, so the area of the gel containing both bands was quantified and expressed as a percentage of total protein (Rad51 + Sfr1). Averages are plotted (n = 3). Error bars depict standard deviation.

significant Rad51 was found in the precipitate when ssDNA was included, and this was largely lost when Fbh1 was added to the reaction, indicating efficient filament disruption by Fbh1. Wildtype S5S1 antagonized this disruption, consistent with previous observations (32), whereas the S5S1-7A mutant was significantly impaired for filament stabilization (Fig. 4, B and D), consistent with previous fluorescence anisotropy experiments (17). Strikingly, S5S1-PM also showed a severe defect in Rad51 filament stabilization against Fbh1-mediated disruption, and this was not observed for S5S1-NON (Fig. 4, C and D). The magnitude of the defect for S5S1-PM was comparable to S5S1-7A (Fig. 4D), indicating that these phosphomimetic mutations in Sfr1 severely impair the stabilization of Rad51 filaments by S5S1.

Stimulation of Rad51-driven strand exchange is compromised by phosphomimetic mutations in Sfr1

Next, we sought to examine whether the defect of S5S1-PM in filament stabilization translated to an impairment in the stimulation of Rad51-driven DNA strand exchange. A strand exchange assay with plasmid-sized DNA substrates was employed to directly test this (Fig. 5A). In this assay, the Rad51 filament is formed on circular ssDNA (cssDNA) and homologous linear dsDNA (ldsDNA) is added. Rad51 drives the pairing of cssDNA and ldsDNA, forming joint molecules (JMs), which are the reaction intermediates. Following strand transfer over the length of the DNA, linear ssDNA and nicked circular DNA (NC) are generated as the reaction products. This assay requires the eukaryotic ssDNA-binding protein RPA (7), which was also purified to homogeneity (Fig. S1A).

We first confirmed that the hexahistidine tag introduced at the N terminus of Sfr1 did not affect the ability of S5S1 to stimulate Rad51-driven strand exchange (Fig. S2). In the absence of S5S1, virtually no JM or NC was observed, indicating that Rad51 is unable to drive homologous DNA pairing and subsequent strand exchange under these conditions (Fig. 5B). The inclusion of substoichiometric amounts of S5S1 strongly stimulated Rad51 activity, with peak stimulation observed at approximately 0.5 μ M (S5S1:Rad51 of 1:10). This stimulatory effect was diminished at higher concentrations, with significantly less NC observed at 2 μ M (and even less at stoichiometric concentrations, see below). This is consistent with previous observations (7, 8, 17). Strikingly, the stimulation of Rad51 by S5S1-PM was severely impaired, with ≥ 2 μ M protein required to achieve stimulation comparable to that of wildtype at 0.5 μ M (Fig. 5B). Given that S5S1-NON showed a stimulation profile that is indistinguishable from wildtype, these results strongly suggest that the introduction of phosphomimetic mutations rather than the loss of S/T residues in Sfr1 compromises the stimulation of Rad51 by S5S1.

Since the results with S5S1-PM are reminiscent of previous observations with S5S1-7A, the established Rad51 interaction mutation, the two mutants were compared to each other side-by-side over a broader concentration range. Consistent with previous observations, S5S1-7A showed peak Rad51 stimulation at 2 to 5 μ M, with only a marginal reduction in

stimulation at 10 μ M; this is in stark contrast to wildtype, where a substantial loss of stimulation was seen even at 5 μ M (Fig. 6A). In the strand exchange assays conducted thus far, Rad51 filaments were allowed to form on ssDNA before the inclusion of S5S1, then RPA was added to facilitate the reaction. To more closely mimic the physiological condition, we changed the order of addition to precoat the ssDNA with RPA, then added Rad51 and S5S1. Even under these conditions, S5S1-7A and S5S1-PM were severely impaired for Rad51 stimulation, whereas S5S1-NON behaved similarly to wildtype S5S1 (Fig. 6B). Overall, the defect in strand exchange stimulation observed for S5S1-PM was very similar to S5S1-7A, though perhaps slightly less severe. Taken together, these results suggest that phosphorylation of Sfr1 at these five residues significantly impairs the ability of S5S1 to stimulate Rad51-driven DNA strand exchange.

In addition to an impairment in the interaction with Rad51, S5S1-7A was previously shown to have severe defects in DNA binding, although, based on multiple lines of indirect evidence, the authors argued that this DNA binding activity may be impertinent to the role of S5S1 in DNA repair (17). Nevertheless, we examined the ability of S5S1-PM to bind DNA in electrophoretic mobility shift assays. Unlike S5S1-7A, S5S1-PM was able to shift both ssDNA (Fig. S3A) and dsDNA (Fig. S3B) significantly, although not to the same extent as wildtype S5S1. Importantly, S5S1-NON shifted DNA comparably to wildtype across all concentrations examined. These results indicate that the introduction of phosphomimetic residues mildly impairs DNA binding. Despite the clear difference in DNA binding between S5S1-7A and S5S1-PM, the fact that both mutants are similarly defective for filament stabilization (Figs. 3 and 4) and strand exchange stimulation (Figs. 5 and 6) is consistent with the notion that the DNA binding activity of S5S1 is not important for Rad51 potentiation (17).

The phosphorylation status of Sfr1 is important for DNA repair

Our biochemical analyses suggested that phosphorylation of Sfr1 severely impairs the S5S1-Rad51 interaction. However, it remained unclear whether this constitutes a physiological mechanism to regulate recombinational DNA repair. To test this, we constructed *S. pombe* strains in which the native *sfr1*⁺ gene was replaced with an allele encoding phosphomimetic D substitutions [*sfr1-PM(D)*] or E substitutions [*sfr1-PM(E)*] at the five S/T residues of interest. A strain encoding the non-phosphorylatable mutant (*sfr1-NON*) was also constructed. These strains were then assayed for DNA damage sensitivity *via* a standard spot-test. *S. pombe* possesses an alternative ultraviolet light (UV) damage repair pathway that requires HR for the repair of endonuclease-induced DNA breaks; the response to UV damage is therefore a suitable measure of HR proficiency (34). In contrast to the strain in which the *sfr1*⁺ gene was deleted (*sfr1 Δ*), the phosphomutants showed normal or near-normal growth following acute exposure to UV, suggesting that DNA repair is not obviously perturbed in these strains (Fig. 7A).

Phosphoregulation of the Rad51 auxiliary factor Swi5-Sfr1

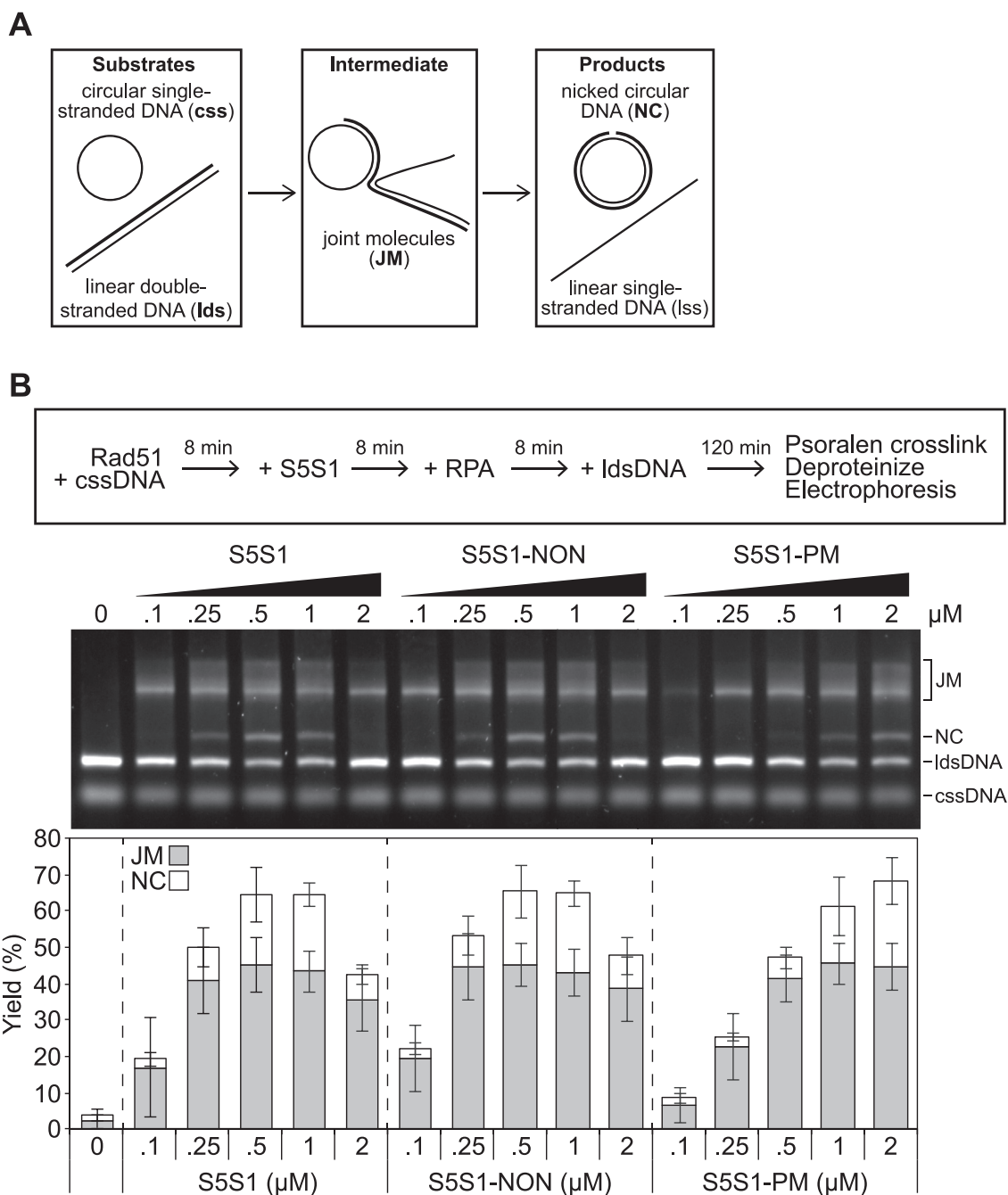
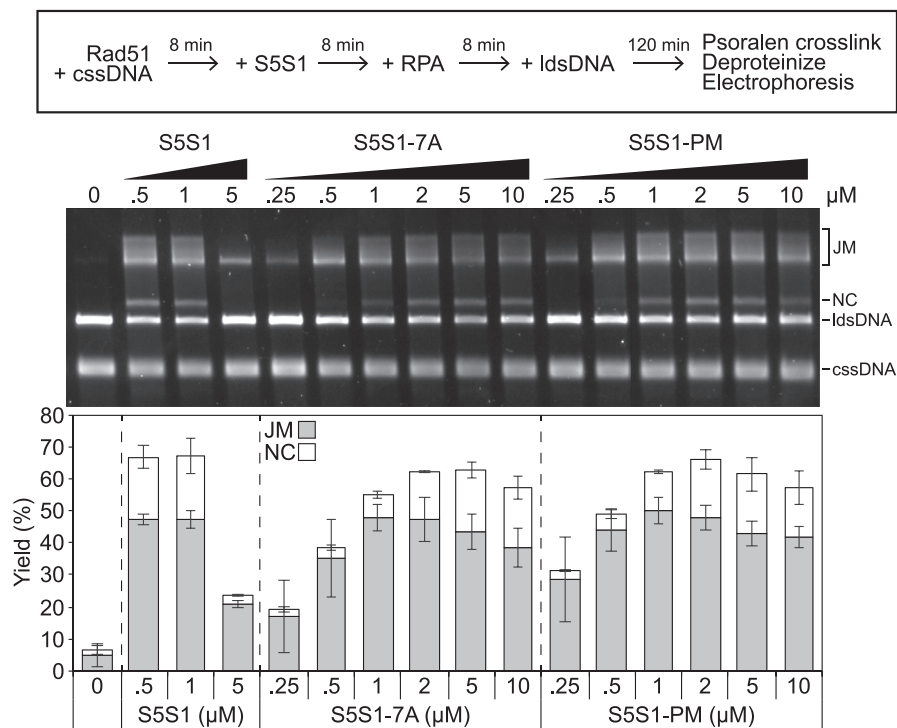


Figure 5. Phosphomimetic mutations in *Sfr1* impair the stimulation of Rad51-driven DNA strand exchange by S5S1. A, schematic of the strand exchange assay. B, all incubations were at 37 °C. Rad51 (5 μM) was incubated with cssDNA (10 μMnt) then supplemented with the indicated concentration of a S5S1 variant. RPA (1 μM) was then added, and following a further incubation, reactions were initiated through the addition of ldsDNA (10 μMnt). After a 2 h incubation, reactions were psoralen-UV crosslinked and deproteinized, and then DNA species were resolved by agarose gel electrophoresis and visualized. Percentage of JM (reaction intermediate) and NC (reaction products) were quantified, and averages were plotted. $n = 6$. Error bars represent standard deviation. cssDNA, circular ssDNA; JM, joint molecule; ldsDNA, linear dsDNA; NC, nicked circular; RPA, replication protein A.

Given the biochemical defects observed for S5S1-PM, this result may seem surprising. However, through examination of the *sfr1-7A* mutant, it was previously shown that Rad55-Rad57 can suppress defects in the interaction of S5S1 with Rad51 (17). With this in mind, we next examined the DNA damage sensitivity of the phosphomutants in the *rad55* Δ background, where the remaining Rad51-dependent DNA repair is strictly dependent on S5S1 (6). Unlike the mild phenotypes of the *sfr1* Δ and *rad55* Δ mutants, the *rad55* Δ *sfr1* Δ double mutant

displayed severe DNA damage sensitivity, as expected based on previous work (6, 35). Strikingly, and in stark contrast to the DNA repair proficiency observed in the presence of Rad55 (Fig. 7A), both phosphomimetic mutants showed similar sensitivity to *sfr1* Δ in the *rad55* Δ background (Fig. 7B). Interestingly, the *sfr1-NON* mutant also displayed a clear sensitivity to DNA damage in the *rad55* Δ background, although this was not as severe as the phosphomimetic mutants. Given that both phosphomimetic mutants phenocopied

A



B

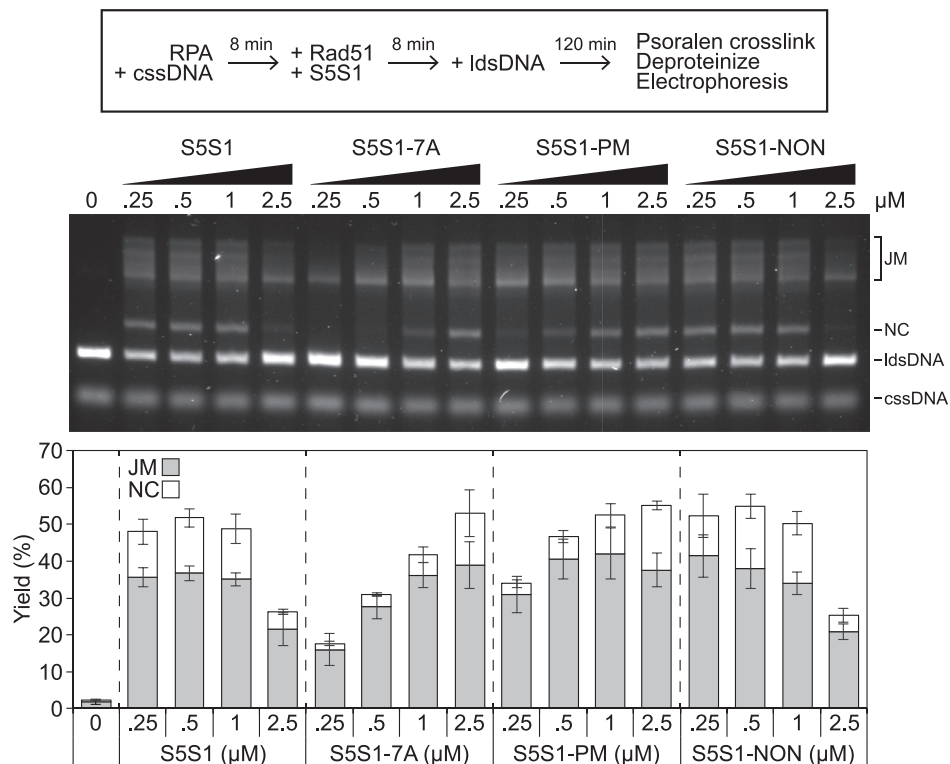


Figure 6. The defects of S5S1-PM in strand exchange stimulation are almost as severe as S5S1-7A. A, the assay was conducted exactly as in Figure 5B, with the indicated concentrations of S5S1. B, all incubations were at 37 °C. RPA (0.33 μM) was first incubated with cssDNA (10 μM nt). Rad51 (5 μM), and the indicated concentration of a S5S1 variant were then added, and following a further incubation, reactions were initiated through the addition of IdsDNA (10 μM nt). After a 2 h incubation, reactions were psoralen-UV crosslinked and deproteinized, then DNA species were resolved by agarose gel electrophoresis and visualized. Percentage of JM (reaction intermediate) and NC (reaction products) were quantified, and averages were plotted. n = 3. Error bars represent standard deviation. cssDNA, circular ssDNA; JM, joint molecule; IdsDNA, linear dsDNA; NC, nicked circular; RPA, replication protein A.

Phosphoregulation of the Rad51 auxiliary factor Swi5–Sfr1

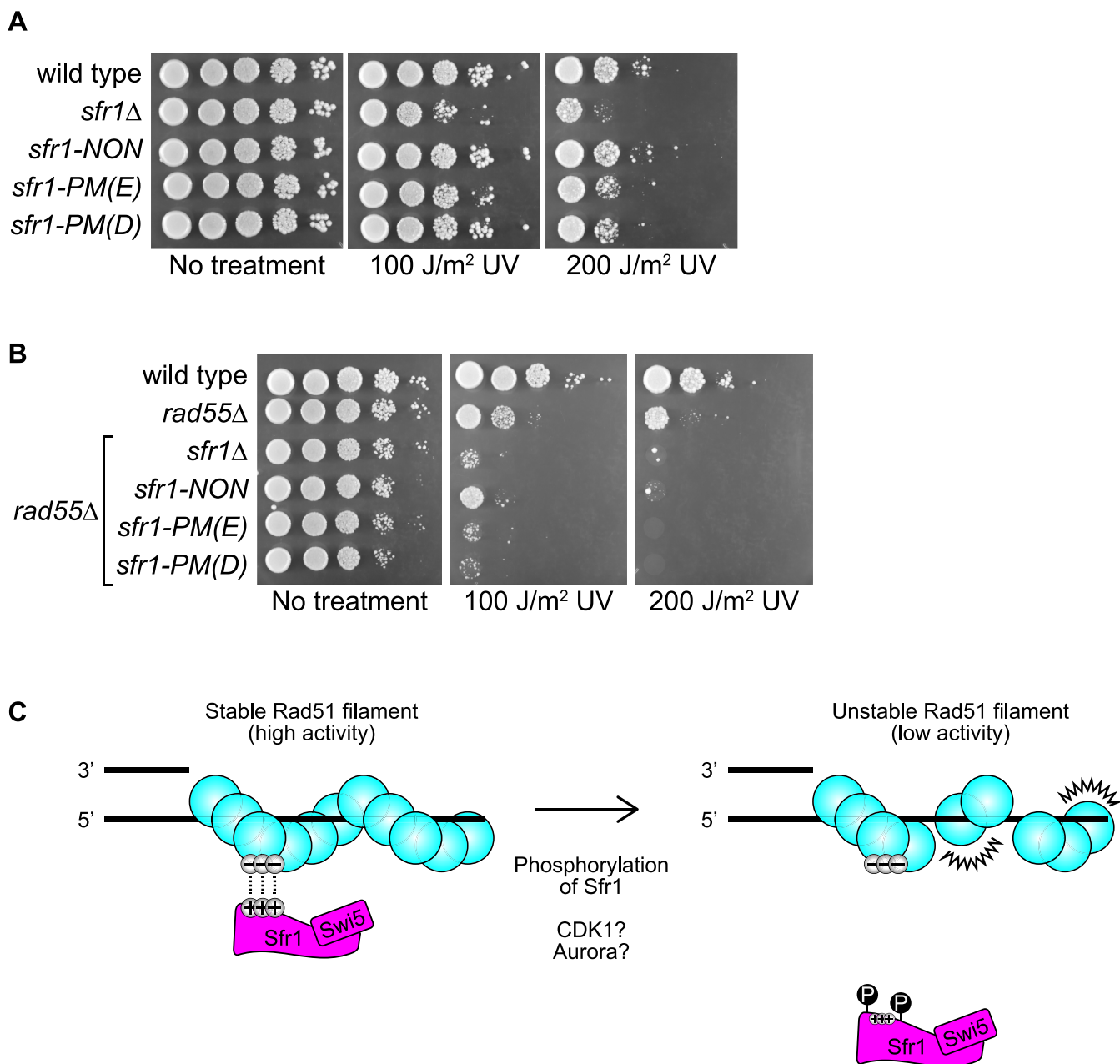


Figure 7. The phosphorylation status of Sfr1 is pertinent for the role of S5S1 in promoting Rad51-dependent DNA repair. A and B, log phase cultures of the indicated *S. pombe* strains were serially diluted (10-fold) and spotted onto solid rich media. Plates were untreated (control) or subjected to the indicated dose of acute UV irradiation, then imaged following growth at 30 °C for 3 to 4 days. Strain numbers and full genotypes are listed in [Experimental procedures](#). C, working model depicting how S5S1 binds to Rad51 and promotes DNA repair.

the previously established Rad51 interaction mutant (*i.e.*, *sfr1-7A*), these results strongly suggest that phosphorylation serves to weaken the S5S1–Rad51 interaction and downregulate recombinational DNA repair, while also pointing toward a potentially complex regulatory mechanism in which abolishing phosphorylation is also detrimental to DNA repair.

Discussion

The potentiation of Rad51 by S5S1 is known to involve binding through two sites in the intrinsically disordered N-terminal half of Sfr1 (17). Furthermore, emerging evidence

has suggested that PTMs play an important role in regulating HR (19). Here, we examined the intersection of these two phenomena. We demonstrated that phosphomimetic mutations in Sfr1 do not obviously affect the global structure of S5S1 or the disordered nature of Sfr1N (Fig. 1). The physical binding of S5S1 to Rad51 was severely reduced by these mutations (Fig. 2), and this resulted in a defect in Rad51 filament stabilization (Figs. 3 and 4), which translated to impaired stimulation of DNA strand exchange (Figs. 5 and 6). Mutant strains of *S. pombe* expressing phosphomimetic Sfr1 showed defects in DNA repair, but only in the absence of Rad55–Rad57 (Fig. 7), consistent with previous suggestions that defects in the

S5S1-Rad51 interaction can be suppressed by Rad55-Rad57 (17). Importantly, the biochemical defects and DNA damage sensitivity phenotypes were comparable to a previously established Rad51 interaction mutant, providing further support for the notion that phosphorylation of Sfr1 is a critical regulator of S5S1-dependent Rad51 modulation. The implications of these findings are discussed below.

Phosphoregulation of the S5S1-Rad51 interaction

Intrinsically disordered regions of proteins are enriched in phosphosites that often regulate their binding to interacting partners, and some phosphorylation events have even been suggested to induce folding of disordered regions (25, 26). A notable example involves the human tri-nuclease complex consisting of SLX1-SLX4, MUS81-EME, and XPF-ERCC1, which is responsible for the nucleolytic processing of a broad range of recombination and replication intermediates (36). The domain of SLX4 that binds MUS81 was shown to be disordered, and significantly, this domain underwent a disorder-to-order transition upon phosphorylation by CDK1 that enhanced its binding to MUS81 (37).

Given that the CD spectra of S5S1-PM and Sfr1N-PM were indistinguishable from wildtype, phosphorylation-induced conformational changes are unlikely to be responsible for the impaired binding of S5S1-PM to Rad51. We favor a scenario where the S5S1-Rad51 interaction involves multiple electrostatic contacts, and the negative charge imparted by phosphorylation, which is mimicked by phosphomimetic mutations, disrupts these contacts. This possibility is supported by several lines of evidence. First, the interaction of Sfr1N with Rad51 displayed clear sensitivity to salt; while Sfr1N coimmunoprecipitated with Rad51 at 25 mM NaCl, this interaction was significantly diminished at 50 mM NaCl (16). Second, mutation of seven positively charged residues (K/R) to A in the two interaction sites of Sfr1N disrupted the binding of S5S1 to Rad51 (17). Third, mutation of three negatively charged residues (D/E) to A on the exterior of the Rad51 filament reproducibly reduced S5S1 binding, albeit mildly (38). We propound that positively charged sites on Sfr1 form contacts with negatively charged sites on Rad51 (Fig. 7C); the addition of negatively charged phosphate groups to Sfr1 likely masks the positively charged sites and impairs binding of S5S1 to Rad51, essentially mimicking the S5S1-7A mutant in which positive residues are neutralized *via* mutation to A.

What kinase could be responsible for this phosphorylation? Among the five S/T residues under examination, four (T73, S109, S116, S165) match the minimal consensus sequence for CDK1 (S/T-P) (39). By contrast, S24 may be phosphorylated by Aurora kinase, another M phase regulator (40). Both S109 and S165 have been shown to be phosphorylated in M phase, when CDK1 activity is at its peak (24). Moreover, using a conditional mutant of CDK1, it was shown that the phosphorylation of S165 was significantly reduced shortly after CDK1 inhibition, with the authors concluding that this phosphorylation is likely to be direct (23). Less is known about the nature of T73 and S165 phosphorylation but given that phosphosites on the same

polypeptide are more likely to be modified with similar timing (23), it is plausible that these sites are also modified by CDK1 in M phase, resulting in a phosphorylated form of S5S1 that is less able to potentiate Rad51 during M phase. This may be required to curb Rad51 activity to reduce the formation of recombination intermediates that may otherwise pose an obstacle to chromosome segregation (41, 42). In the absence of such a regulatory mechanism, genome instability would ensue, leading to increased DNA damage sensitivity, as observed for the *sfr1-NON* mutant. Alternatively, it is possible that phosphorylation of Sfr1 is required to promote the dissociation of S5S1 from Rad51 after strand invasion/exchange to prevent unproductive interactions that may hinder downstream steps of HR. Presently, it is not possible to distinguish between these two possibilities. Additional support for the involvement of CDK1 in regulating S5S1 comes from the observation that genetic interactions exist between *sfr1*⁺ and the CDK activating kinase *csk1*⁺, with the authors suggesting that Csk1 may act *via* CDK1 to influence HR (43). Given the complex nature of these genetic interactions, it is likely that the underlying mechanisms are intricate and multitiered.

Swi5–Sfr1 is evolutionarily conserved and promotes HR in both mice and humans (9, 10). Although there are no reports detailing the biochemical properties of human SWI5-SFR1, extensive analysis of the mouse complex has indicated that the mechanisms through which it potentiates Rad51—namely stabilization of Rad51 filaments and the stimulation of Rad51's ATPase activity (11–13, 29)—are largely conserved with *S. pombe* Swi5–Sfr1 (14, 33). However, intrinsically disordered domains are more tolerant to mutations than structured regions and consequently accumulate mutations at a higher rate (44). Although Sfr1N shows high sequence divergence (17), we nevertheless performed sequence alignments to glean insights into whether the phosphosites examined here might be evolutionarily conserved.

Within the *Schizosaccharomyces* genus, we made several potentially interesting observations (Fig. S4A): S109 and S165 were conserved in all species; S116 was partially conserved (a T residue in every other species); and T73 was only conserved in *Schizosaccharomyces japonicus*. Given that S109 and S165 were completely conserved within the *Schizosaccharomyces* genus, we postulate that these two residues are central to the phosphoregulation of Sfr1. It would be interesting to compare a variant of S5S1 in which only these two sites are mutated to phosphomimetic residues. When compared to mouse SWI5-SFR1, S24 was conserved and T73 was partially conserved (S in mouse) (Fig. S4B). Interestingly, S116 was replaced with a nonphosphorylatable A residue and S165 was replaced with a phosphomimetic E residue. No conservation was observed with human SWI5-SFR1, with the only notable observation being that S109 was replaced with a phosphomimetic E residue (Fig. S4C). It remains to be determined whether these similarities/differences are of functional significance.

In addition to phosphorylation of Sfr1, *S. pombe* Rad51 is ubiquitylated by both Fbh1, an F-box family helicase, and Rrp1, a RING-domain containing SWI/SNF-family translocase (32, 45). It is not known whether these modifications affect

Phosphoregulation of the Rad51 auxiliary factor Swi5–Sfr1

Rad51 activity and their relation (if any) to Sfr1 phosphorylation. What is becoming increasingly clear is that PTM of HR factors plays critical roles in modulating recombinational DNA repair (19). Mechanistically, this may be achieved through the regulation of Rad51 binding potential, as demonstrated here for S5S1.

Interplay between S5S1 and Rad55–Rad57

In *S. pombe*, the mild sensitivity of the *rad55Δ* (or *rad57Δ*) and *swi5Δ* (or *sfr1Δ*) single mutants compared with the severe sensitivity of the double mutant—which resembles the *rad51Δ* single mutant—was interpreted to mean that Rad55–Rad57 and Swi5–Sfr1 function in independent subpathways of HR (6, 35). However, this was challenged by the discovery that defects in the S5S1–Rad51 interaction are suppressed by a Rad55–Rad57–dependent mechanism and that S5S1 and Rad55–Rad57 physically interact with each other (17). Interestingly, S5S1 suppressed the defects of the *rad51-E206A* mutant, which was suggested to be specifically defective in the interaction with Rad55–Rad57 (38). Collectively, these findings led to the proposal that, although capable of functioning independently of each other, Rad55–Rad57 and S5S1 collaboratively promote Rad51-dependent DNA repair in wildtype cells (17, 38).

When combined with our biochemical analyses indicating that S5S1-PM is defective in the physical and functional interaction with Rad51, the demonstration that *sfr1-PM(D)* and *sfr1-PM(E)* phenocopy *sfr1-7A* provides further support for the existence of interplay between Rad55–Rad57 and S5S1. How Rad55–Rad57 suppresses the defects of S5S1-7A and S5S1-PM is unclear. Given that Rad55–Rad57 can interact with both Rad51 and S5S1, it was proposed that Rad55–Rad57 can function as a molecular bridge to increase the local concentration of S5S1-7A around Rad51, thereby allowing S5S1C to stimulate Rad51 (17). A reasonable inference that can be drawn from the suppression of *sfr1-NON* by Rad55 is that the DNA repair defects in this strain are also associated with a dysregulated Rad51 interaction. We hypothesize that in the cellular context, S5S1-NON interacts with Rad51 with increased affinity compared to wildtype S5S1, which may exist in a partially phosphorylated state. This increased affinity likely leads to unproductive/untimely interactions with Rad51 that are detrimental to DNA repair. Interestingly, budding yeast Rad55 is also phosphorylated, and this modification was shown to be important for DNA repair (46, 47). The precise biological requirement for these phosphorylation events, along with the interplay between different auxiliary factors and their PTMs, will likely be a focal point of future research.

Experimental procedures

Protein purification

Rad51 and RPA were purified exactly as previously described (17). N-terminally hexahistidine-tagged Sfr1 was co-expressed with Swi5 as an operon from a pET11b vector in an *E. coli* BL21 DE3 strain (NEB) that had been pretransformed with the pRARE2 plasmid (Novagen). Plasmids used are:

pBA184, S5S1; pBA186, S5S1-NON; pBA187, S5S1-PM; and pBA197, S5S1-7A. For each S5S1 variant, 2 L of *E. coli* was grown to an A600 of 0.4 to 0.5, 1 mM of IPTG was added, and incubation was continued at 18 °C for ~15 h at 170 rpm. Cells were then harvested by centrifugation. All subsequent steps were carried out at 4 °C. Cells (8–10 g wet weight) were resuspended in 50 ml of lysis buffer (25 mM Hepes-KOH [pH 7.5], 500 mM NaCl, 10% glycerol, 0.5 mM TCEP), lysed by sonication, and clarified by centrifugation (67,000g 1 h). Cleared lysates were supplemented with 0.05% polyethyleneimine, incubated for 30 min with mixing, and precipitate was removed by centrifugation (25,000g 20 min). Ammonium sulphate was slowly added to the supernatant (35% saturation), which was then incubated with mixing for 1 h. Precipitate was collected by centrifugation (10,000g 10 min), resuspended in 50 ml of lysis buffer, and applied to a 5 ml cComplete His-tag purification column (Roche). The column was then washed with ~100 ml of lysis buffer, and bound proteins were eluted in 25 ml of lysis buffer supplemented with 300 mM imidazole. The eluate was dialyzed overnight against 1 L of H buffer (25 mM Hepes-KOH [pH 7.5], 10% glycerol, 0.5 mM TCEP) containing 200 mM KCl, diluted with 3× volumes of H buffer, and applied to a HiTrap Q column (5 ml). Proteins were eluted with a linear gradient (100–600 mM KCl, 190 ml). Peak fractions were combined, concentrated to ~3 ml, applied to a 16/60 Superdex 200 pg gel filtration column, and developed in H buffer containing 200 mM KCl. Peak fractions were combined, concentrated, and flash-frozen in liquid nitrogen as small aliquots. Protein concentration was estimated by measuring A280 with a molar extinction coefficient of 12,490 M⁻¹ cm⁻¹.

Up until ammonium sulphate precipitation, N-terminally hexahistidine-tagged Sfr1N (pBA198) and Sfr1N-PM (pBA200) were treated the same as S5S1. Ammonium sulphate precipitation was at 45% saturation. Following nickel affinity purification and dialysis, the sample was applied to a HiTrap Q column (5 ml) and recovered in the flow-through. The sample was then applied to a HiTrap Heparin column (5 ml) and eluted with a linear gradient (100–600 mM KCl, 100 ml). Peak fractions were concentrated, and Sfr1N was further purified by gel filtration, as for Swi5–Sfr1. Protein concentration was estimated by the bicinchoninic acid assay, with wildtype S5S1 serving as a standard. Other than the His-tag purification column, all columns are from Cytiva. Chromatograms for size-exclusion chromatography are shown in Figure 1 and are expressed relative to the highest A280 reading during each run.

Circular dichroism spectroscopy

Global secondary structure was examined using a spectrometer (Chirascan, Applied Photophysics) with a Peltier temperature controller (Quantum Northwest). Swi5–Sfr1 or Sfr1N (wildtype or mutants) were diluted to 7.35 μM in 20 mM potassium phosphate (pH 7.4) and transferred into a 1 mm path length quartz cuvette (Hellma Analytics). Circular dichroism was recorded from 190 to 260 nm at 20

°C (0.5 nm intervals, 1 nm bandwidth, for 1 s per datapoint).

Protein–protein interaction assays

For the in-solution pull-down assay using nickel resin (Fig. 2A), 500 nM of Rad51 was mixed with 500 nM of S5S1 (wildtype or mutant) in pull-down buffer (30 mM Tris-Cl [7.5], 100 mM KCl, 5 mM MgCl₂, 1 mM ATP, 0.25 mM TCEP, 5% glycerol, 0.05% Tween-20) on ice (total volume 120 µl). Ten microliter was withdrawn and mixed with SDS-PAGE loading buffer (input). The remaining reaction was incubated at 30 °C for 15 min then on ice for 5 min. Ten microliter of cOmplete nickel resin (Roche) was added to each reaction, and hexahistidine-tagged proteins were immobilized on the resin by incubating with gentle agitation for 1 h at 4 °C. The resin was pelleted by brief centrifugation and washed twice with 400 µl of pull-down buffer. Bound proteins were eluted with 40 µl of SDS-PAGE loading buffer (37 °C 10 min 1300 rpm) and analyzed by SDS-PAGE.

For the filament binding assay (Fig. 2C), 3.33 µM Rad51 was added to filament binding buffer (25 mM Tris-Cl [7.5], 100 mM NaCl, 3.5 mM MgCl₂, 2 mM ATP, 0.5 mM TCEP, 5% glycerol, 0.05% Tween-20) containing 10 µMnt of circular ssDNA (PhiX174 virion DNA, NEB) immobilized on magnetic Streptavidin-coated beads (Dynabeads M-280, ThermoFisher Scientific) through an oligonucleotide with a biotin moiety at its 5' end (BA655, ATAAGGCCACGTATTTTGCAAGCTATTTAACTGGCGGCGATTGCGTACCCGACGACCAAATTAGGGTCAACGCTACCTGTAGGAAGTGTCCGCATAAAG). Filaments were allowed to form by incubating at 37 °C with gentle agitation for 5 min, then 3.33 µM S5S1 (wildtype or mutant) was added, and incubation was continued as before for a further 5 min. The solution was then separated into precipitate (DNA bound) and supernatant (unbound) fractions using a magnetic stand. Proteins were eluted from the resin in 1x SDS-PAGE loading buffer (37 °C 15 min 1300 rpm) and, along with the supernatant fraction, analyzed by SDS-PAGE. Bound proteins were quantified in FIJI (48). Briefly, background was subtracted using the rolling ball method, then the signal corresponding to the region of the gel containing Sfr1 for the reaction where Sfr1 was omitted was subtracted from the corresponding signal for reactions containing Sfr1. Sfr1 signal was then normalized to Rad51 and plotted relative to wildtype (n = 3).

Negative stain electron microscopy

Electron microscopy buffer (25 mM Hepes-KOH [pH 7.5], 100 mM KCl, 2 mM ATP, 5 mM MgCl₂, 0.5 mM TCEP) containing 1.5 µMnt of a 116-mer oligonucleotide (BA494, TTCAATATCTGGTTGAACGGCGTCGCGTCGTAACCCAGCTTGGTAAGTTGGATTAAGCACTCCGTGGACAGATTTGTCATTGTGAGCATTTTCATCCCGAAGTTGCGGCTCATTCT) was supplemented with Rad51 (500 nM) and incubated at 37 °C for 5 min. Swi5–Sfr1 (wildtype or mutants, 100 nM) was then added, and incubation was continued for 10 min. Four microliters of the reaction was then applied to a carbon-coated 300 mesh copper grid (Agar

Scientific) and fixed with 2% uranyl acetate. Images were captured using a Tecnai 12 electron microscope at 52,000× magnification, and filament length was measured using FIJI (48). Visualization and statistical analysis was performed in GraphPad Prism (version 8).

Fbh1-mediated filament disruption assay

All concentrations indicate final concentrations in the 10 µl reaction, and all incubations were at 37 °C. Filament disruption buffer (25 mM Tris-Cl [pH 7.5], 100 mM NaCl, 2 mM ATP, 5 mM MgCl₂, 0.5 mM TCEP, 5% glycerol, 0.2% Tween-20, 6 mM phosphocreatine, 6 U/ml creatine kinase) containing 10 µMnt of a 5'-biotinylated 100-mer oligonucleotide (BA655, ATAAGGCCACGTATTTTGCAAGCTATTTAACTGGCGGCGATTGCGTACCCGACGACCAAATTAGGGTCAACGCTACCTGTAGGAAGTGTCCGCATAAAG) was supplemented with Rad51 (3.33 µM) and incubated for 7 min. The indicated concentration of a Swi5–Sfr1 variant was added, and reactions were incubated for a further 7 min. To disrupt filaments, Fbh1 (0.312 µM) was added and incubation continued for 10 min. Ten microliter of streptavidin-coated magnetic beads (Dynabeads M280, Thermo Fisher Scientific) was then added, followed by a further 15 min incubation (1300 rpm). A magnetic tube rack was then used to separate the beads from the supernatant. Beads were then resuspended in SDS-PAGE loading buffer and bound proteins eluted (10 min 1300 rpm). Both supernatant and precipitate fractions (in SDS-PAGE loading buffer) were heated (65 °C 5 min), then proteins were analyzed by SDS-PAGE and Coomassie staining. Following sufficient staining and destaining, gels were imaged using the ChemiDoc MP Imaging System (Bio-Rad). Quantification was performed in FIJI (48) by subtracting background signal (rolling ball method), then the signal corresponding to Rad51-Sfr1 in the precipitate was expressed as a percentage of total Rad51-Sfr1 (precipitate + supernatant).

DNA strand exchange assay

All concentrations indicate final concentrations in the 10 µl reaction, and all incubations were at 37 °C. Strand exchange buffer (25 mM Tris-Cl [pH 7.5], 100 mM KCl, 2 mM ATP, 3.5 mM MgCl₂, 0.5 mM TCEP, 5% glycerol, 4 mM phosphocreatine, 4 U/ml creatine kinase) was supplemented with 10 µMnt cssDNA (NEB, PhiX virion DNA). Proteins were then added in the order indicated for each experiment, with concentrations described in respective figure legends. 10 µMnt ldsDNA (NEB, PhiX RF I digested with ApaLI) was added to initiate the strand exchange reaction. After 2 h, 1 µl of 200 µg/ml psoralen was added, and the reactions were exposed to 200 µJ/cm² UV (UVP, CL-1000 ultraviolet crosslinker). Reactions were then deproteinized through the addition of 2.5 µl stop solution (120 mM Tris-Cl, 60 mM EDTA, 1% SDS, 0.77 mg/ml proteinase K) and incubation for 15 min at 37 °C. Reactions were separated by agarose gel electrophoresis, and DNA was visualized by staining with SYBR Gold (Thermo Fisher Scientific). Images were captured using the ChemiDoc MP Imaging System (Bio-Rad). Quantification was performed

Phosphoregulation of the Rad51 auxiliary factor Swi5–Sfr1

in FIJI (48) by subtracting background signal (rolling ball method), then the signal corresponding to NC was expressed as a percentage of the total lane signal (sum of ldsDNA, JM divided by 1.5, NC). For JM, the signal was divided by 1.5 and then expressed as a percentage of the total lane signal.

Electrophoretic mobility shift assay

DNA binding buffer (25 mM Hepes-KOH [pH 7.5], 100 mM KCl, 3.5 mM MgCl₂, 0.5 mM TCEP, 5% glycerol) containing 20 nM ssDNA with a Cy5 label at the 3' end (80-mer, BA663: TTGATAAGAGGTCATTTTTGCGGATGGCTTAGAGCTT AATTGCTGAATCTGGTGCTGTAGCTCAACATGTTTTA AATATG), or BA663 annealed to its unlabeled complementary strand (BA664), was supplemented with the denoted concentration of Swi5–Sfr1 (wildtype or mutants) in a 10 μ l reaction. After a 15 min incubation at 37 °C, 2 μ l of loading dye was added to the reaction, and samples were separated by agarose gel electrophoresis at 4 °C (0.8% gel in TAE buffer). Gels were imaged using a ChemiDoc MP Imaging System (Bio-Rad). Oligonucleotides were synthesized by Eurofins and purified by HPLC.

Spot-test to assay DNA damage sensitivity

S. pombe strains were prepared by tetrad dissection according to standard protocols (49), and spot-tests were conducted exactly as previously described (38). Briefly, single colonies were inoculated in rich media (YE with supplements) for 24 h, then diluted into fresh media and grown until they reached a cell density of approximately 1×10^7 cells/ml. Ten-fold serial dilutions were then prepared, and 5 μ l of cells were spotted onto solid rich media, with the most concentrated spot corresponding to 1×10^5 cells. Plates were either untreated (control) or exposed to the indicated dose of ultraviolet light, then left for 3 to 4 days until sufficient growth was observed. Growth was always at 30 °C. Strains used in Figure 7A are: BA196 (*sfr1*⁺-*kanMX6*), BA125 (*sfr1::kanMX6*), BA215 (*sfr1-NON-kanMX6*), BA240 (*sfr1-PM[E]-kanMX6*), and BA243 (*sfr1-PM[D]-kanMX6*). Strain used in Figure 7B are: BA53 (wildtype), BA194 (*rad55::natMX6 sfr1*⁺-*kanMX6*), BA126 (*rad55::arg3 sfr1::kanMX6*), BA252 (*rad55::natMX6 sfr1-NON-kanMX6*), BA260 (*rad55::natMX6 sfr1-PM[E]-kanMX6*), and BA256 (*rad55::natMX6 sfr1-PM[D]-kanMX6*). All strains are isogenic derivatives of BA53 (*h-mat1M smt0 ura4-D18 leu1-32 his3-D1 arg3-D1*).

Data availability

There are no data to be deposited in databases. All relevant data have been included in the manuscript.

Supporting information—This article contains supporting information.

Acknowledgments—We would like to thank all members of our laboratory for support and discussions, as well as Marc Morgan of the Protein Crystallography and Macromolecular Interactions Facilities for help with circular dichroism experiments. B.A. also

extends his gratitude to Hiroshi Iwasaki (Tokyo Institute of Technology) for support during the early stages of the project.

Author contributions—P. L., K. L., and B. A. validation; P. L., K. L., L. Y., B. A., and X. Z. formal analysis; P. L., K. L., L. Y., and B. A. investigation; P. L., K. L., B. A., and X. Z. resources; P. L., K. L., L. Y., B. A., and X. Z. writing—review & editing; P. L., K. L., and B. A. visualization; L. Y., B. A., and X. Z. conceptualization; L. Y. and B. A. methodology; L. Y., B. A., and X. Z. supervision; B. A. and X. Z. writing—original draft; B. A. and X. Z. project administration; B. A. and X. Z. funding acquisition.

Funding and additional information—This work was supported by a Marie Skłodowska-Curie Actions fellowship to B. A. (101022335) and a Wellcome Trust Senior Investigator Award to X. Z. (210658/Z/18/Z).

Conflict of interest—The authors declare that they have no conflicts of interest with the contents of this article.

Abbreviations—The abbreviations used are: CD, circular dichroism; cssDNA, circular ssDNA; D-loop, displacement loop; DSB, double-strand break; dsDNA, double-stranded DNA; HR, homologous recombination; JM, joint molecule; ldsDNA, linear dsDNA; NC, nicked circular; NSEM, negative-stain electron microscopy; PTM, posttranslational modifications; RPA, replication protein A; S5S1, Swi5–Sfr1; S5S1C, Swi5–Sfr1C; ssDNA, single-stranded DNA.

References

1. Mehta, A., and Haber, J. E. (2014) Sources of DNA double-strand breaks and models of recombinational DNA repair. *Cold Spring Harb. Perspect. Biol.* **6**, a016428
2. Symington, L. S., and Gautier, J. (2011) Double-strand break end resection and repair pathway choice. *Annu. Rev. Genet.* **45**, 247–271
3. Sun, Y., McCorvie, T. J., Yates, L. A., and Zhang, X. (2020) Structural basis of homologous recombination. *Cell. Mol. Life Sci.* **77**, 3–18
4. Greene, E. C. (2016) DNA sequence alignment during homologous recombination. *J. Biol. Chem.* **291**, 11572–11580
5. Haber, J. E. (2018) DNA repair: the search for homology. *BioEssays* **40**, e1700229
6. Akamatsu, Y., Dziadkowiec, D., Ikeguchi, M., Shinagawa, H., and Iwasaki, H. (2003) Two different Swi5-containing protein complexes are involved in mating-type switching and recombination repair in fission yeast. *Proc. Natl. Acad. Sci. U. S. A.* **100**, 15770–15775
7. Haruta, N., Kurokawa, Y., Murayama, Y., Akamatsu, Y., Unzai, S., Tsutsui, Y., et al. (2006) The Swi5–Sfr1 complex stimulates Rhp51/Rad51- and Dmc1-mediated DNA strand exchange *in vitro*. *Nat. Struct. Mol. Biol.* **13**, 823–830
8. Kurokawa, Y., Murayama, Y., Haruta-Takahashi, N., Urabe, I., and Iwasaki, H. (2008) Reconstitution of DNA strand exchange mediated by Rhp51 recombinase and two mediators. *PLoS Biol.* **6**, e88
9. Akamatsu, Y., and Jasin, M. (2010) Role for the Mammalian Swi5–Sfr1 Complex in DNA strand break repair through homologous recombination. *PLoS Genet.* **6**, e1001160
10. Yuan, J., and Chen, J. (2011) The Role of the Human SWI5–MEI5 complex in homologous recombination repair. *J. Biol. Chem.* **286**, 9888–9893
11. Tsai, S.-P., Su, G.-C., Lin, S.-W., Chung, C.-I., Xue, X., Dunlop, M. H., et al. (2012) Rad51 presynaptic filament stabilization function of the mouse Swi5–Sfr1 heterodimeric complex. *Nucleic Acids Res.* **40**, 6558–6569
12. Su, G.-C., Chung, C.-I., Liao, C.-Y., Lin, S.-W., Tsai, C.-T., Huang, T., et al. (2014) Enhancement of ADP release from the RAD51 presynaptic filament by the SWI5–SFR1 complex. *Nucleic Acids Res.* **42**, 349–358

13. Su, G.-C., Yeh, H.-Y., Lin, S.-W., Chung, C.-I., Huang, Y.-S., Liu, Y.-C., *et al.* (2016) Role of the RAD51-SWI5-SFR1 Ensemble in homologous recombination. *Nucleic Acids Res.* **44**, 6242–6251
14. Argunhan, B., Murayama, Y., and Iwasaki, H. (2017) The differentiated and conserved roles of Swi5-Sfr1 in homologous recombination. *FEBS Lett.* **591**, 2035–2047
15. Kokabu, Y., Murayama, Y., Kuwabara, N., Oroguchi, T., Hashimoto, H., Tsutsui, Y., *et al.* (2011) Fission yeast Swi5-Sfr1 protein complex, an activator of Rad51 recombinase, forms an extremely elongated dogleg-shaped structure*. *J. Biol. Chem.* **286**, 43569–43576
16. Kuwabara, N., Murayama, Y., Hashimoto, H., Kokabu, Y., Ikeguchi, M., Sato, M., *et al.* (2012) Mechanistic insights into the activation of Rad51-mediated strand exchange from the structure of a recombination activator, the Swi5-Sfr1 complex. *Structure* **20**, 440–449
17. Argunhan, B., Sakakura, M., Afshar, N., Kurihara, M., Ito, K., Maki, T., *et al.* (2020) Cooperative interactions facilitate stimulation of Rad51 by the Swi5-Sfr1 auxiliary factor complex. *Elife* **9**, e52566
18. Sung, P., Krejci, L., Komen, S. V., and Sehorn, M. G. (2003) Rad51 recombinase and recombination mediators. *J. Biol. Chem.* **278**, 42729–42732
19. Argunhan, B., Iwasaki, H., and Tsubouchi, H. (2021) Post-translational modification of factors involved in homologous recombination. *DNA Repair (Amst)* **104**, 103114
20. Cipak, L., Spirek, M., Novatchkova, M., Chen, Z., Rumpf, C., Lugmayr, W., *et al.* (2009) An improved strategy for tandem affinity purification-tagging of *Schizosaccharomyces pombe* genes. *Proteomics* **9**, 4825–4828
21. Carpy, A., Krug, K., Graf, S., Koch, A., Popic, S., Hauf, S., *et al.* (2014) Absolute proteome and phosphoproteome dynamics during the cell cycle of *Schizosaccharomyces pombe* (Fission Yeast)*. *Mol. Cell. Proteomics* **13**, 1925–1936
22. Kettenbach, A. N., Deng, L., Wu, Y., Baldissard, S., Adamo, M. E., Gerber, S. A., *et al.* (2015) Quantitative phosphoproteomics reveals pathways for coordination of cell growth and division by the conserved fission yeast kinase Pom1*. *Mol. Cell. Proteomics* **14**, 1275–1287
23. Swaffer, M. P., Jones, A. W., Flynn, H. R., Snijders, A. P., and Nurse, P. (2016) CDK Substrate phosphorylation and ordering the cell cycle. *Cell* **167**, 1750–1761.e16
24. Swaffer, M. P., Jones, A. W., Flynn, H. R., Snijders, A. P., and Nurse, P. (2018) Quantitative phosphoproteomics reveals the signaling dynamics of cell-cycle kinases in the fission yeast *Schizosaccharomyces pombe*. *Cell Rep.* **24**, 503–514
25. Oldfield, C. J., and Dunker, A. K. (2014) Intrinsically disordered proteins and intrinsically disordered protein regions. *Annu. Rev. Biochem.* **83**, 553–584
26. Shammas, S. L., Crabtree, M. D., Dahal, L., Wicky, B. I. M., and Clarke, J. (2016) Insights into Coupled folding and binding mechanisms from kinetic studies. *J. Biol. Chem.* **291**, 6689–6695
27. Greenfield, N. J. (2006) Using circular dichroism spectra to estimate protein secondary structure. *Nat. Protoc.* **1**, 2876–2890
28. Mirdita, M., Schütze, K., Moriwaki, Y., Heo, L., Ovchinnikov, S., and Steinegger, M. (2022) ColabFold: making protein folding accessible to all. *Nat. Methods* **19**, 679–682
29. Lu, C.-H., Yeh, H.-Y., Su, G.-C., Ito, K., Kurokawa, Y., Iwasaki, H., *et al.* (2018) Swi5-Sfr1 stimulates Rad51 recombinase filament assembly by modulating Rad51 dissociation. *Proc. Natl. Acad. Sci. U. S. A.* **115**, 201812753
30. Zhao, L., Xu, J., Zhao, W., Sung, P., and Wang, H.-W. (2018) Determining the RAD51-DNA nucleoprotein filament structure and function by cryo-electron microscopy. *Methods Enzymol.* **600**, 179–199
31. Simandlova, J., Zigelbaum, J., Payne, M. J., Chu, W. K., Shevelev, I., Hanada, K., *et al.* (2013) FBH1 helicase disrupts RAD51 filaments *in Vitro* and modulates homologous recombination in mammalian cells. *J. Biol. Chem.* **288**, 34168–34180
32. Tsutsui, Y., Kurokawa, Y., Ito, K., Siddique, M. S. P., Kawano, Y., Yamao, F., *et al.* (2014) Multiple regulation of Rad51-mediated homologous recombination by fission yeast Fbh1. *PLoS Genet.* **10**, e1004542
33. Tsubouchi, H., Argunhan, B., and Iwasaki, H. (2021) Biochemical properties of fission yeast homologous recombination enzymes. *Curr. Opin. Genet. Dev.* **71**, 19–26
34. McCready, S. J., Osman, F., and Yasui, A. (2000) Repair of UV damage in the fission yeast *Schizosaccharomyces pombe*. *Mutat. Res.* **451**, 197–210
35. Akamatsu, Y., Tsutsui, Y., Morishita, T., Siddique, M. S. P., Kurokawa, Y., Ikeguchi, M., *et al.* (2007) Fission yeast Swi5/Sfr1 and Rhp55/Rhp57 differentially regulate Rhp51-dependent recombination outcomes. *EMBO J.* **26**, 1352–1362
36. Wyatt, H. D. M., Laister, R. C., Martin, S. R., Arrowsmith, C. H., and West, S. C. (2017) The SMX DNA repair tri-nuclease. *Mol. Cell* **65**, 848–860.e11
37. Payliss, B. J., Tse, Y. W. E., Reichheld, S. E., Lemak, A., Yun, H. Y., Houlston, S., *et al.* (2022) Phosphorylation of the DNA repair scaffold SLX4 drives folding of the SAP domain and activation of the MUS81-EME1 endonuclease. *Cell Rep.* **41**, 111537
38. Afshar, N., Argunhan, B., Palihati, M., Taniguchi, G., Tsubouchi, H., and Iwasaki, H. (2021) A novel motif of Rad51 serves as an interaction hub for recombination auxiliary factors. *Elife* **10**, e64131
39. Enserink, J. M., and Kolodner, R. D. (2010) An overview of Cdk1-controlled targets and processes. *Cell Div.* **5**, 11
40. Koch, A., Krug, K., Pengelley, S., Macek, B., and Hauf, S. (2011) Mitotic substrates of the kinase aurora with roles in chromatin regulation identified through quantitative phosphoproteomics of fission yeast. *Sci. Signal.* **4**, rs6
41. Chan, Y. W., Fugger, K., and West, S. C. (2017) Unresolved recombination intermediates lead to ultra-fine anaphase bridges, chromosome breaks and aberrations. *Nat. Cell Biol.* **20**, 1–18
42. Tiwari, A., Jones, O. A., and Chan, K.-L. (2018) 53BP1 can limit sister-chromatid rupture and rearrangements driven by a distinct ultrafine DNA bridging-breakage process. *Nat. Commun.* **9**, 677
43. Gerber, H. B., Pikman, Y., and Fisher, R. P. (2008) The CDK-Activating Kinase (CAK) Csk1 is required for normal levels of homologous recombination and resistance to DNA damage in fission yeast. *PLoS One* **3**, e1492–e1499
44. Brown, C. J., Takayama, S., Campen, A. M., Vise, P., Marshall, T. W., Oldfield, C. J., *et al.* (2002) Evolutionary rate heterogeneity in proteins with long disordered regions. *J. Mol. Evol.* **55**, 104–110
45. Muraszko, J., Kramarz, K., Argunhan, B., Ito, K., Baranowska, G., Kurokawa, Y., *et al.* (2021) Rrp1 translocase and ubiquitin ligase activities restrict the genome destabilising effects of Rad51 in fission yeast. *Nucleic Acids Res.* **49**, 6832–6848
46. Bashkurov, V. I., King, J. S., Bashkurova, E. V., Schmuckli-Maurer, J., and Heyer, W. D. (2000) DNA repair protein Rad55 is a terminal substrate of the DNA damage checkpoints. *Mol. Cell. Biol.* **20**, 4393–4404
47. Herzberg, K., Bashkurov, V. I., Rolfmeier, M., Haghazari, E., McDonald, W. H., Anderson, S., *et al.* (2006) Phosphorylation of Rad55 on Serines 2, 8, and 14 is required for efficient homologous recombination in the recovery of stalled replication forks. *Mol. Cell. Biol.* **26**, 8396–8409
48. Schindelin, J., Arganda-Carreras, I., Frise, E., Kaynig, V., Longair, M., Pietzsch, T., *et al.* (2012) Fiji: an open-source platform for biological-image analysis. *Nat. Methods* **9**, 676–682
49. Forsburg, S. L., and Rhind, N. (2006) Basic methods for fission yeast. *Yeast* **23**, 173–183